A novel spectrum filter for fully constrained mixture analysis

MEI Shao-hui, HE Ming-yi

Shaanxi Key Laboratory of Information Acquisition and Processing, School of Electronics and Information, Northwestern Polytechnical University, Shaanxi Xi'an 710129, *China*

Abstract: The presentation of mixtures not only influences the performance of image classification and target recognition, but also is an obstacle to quantitative analysis of remote sensing images. Therefore, a novel spectrum filter based fully constrained mixture analysis algorithm is proposed in this paper to tackle this problem. The spectrum filter, which could wipe off the background spectrum in a mixed pixel, is firstly proposed to obtain the sum-to-one constrained fractional abundance of mixtures in remote sensing images. Since the precise endmember set of a mixture can be obtained by continually modifying the endmember space when minus abundance exists, the spectrum filter based iterative algorithm is present to realize fully constrained mixture analysis. Experimental analysis based on synthetic multispectral data set demonstrates that the proposed algorithm obviously outperforms the popular Fully Constrained Least Square unmixing (FCLS) algorithm and the Orthogonal Subspace Projection (OSP) algorithm. In addition, the proposed algorithm also achieves very promising performance on real hyperspectral images.

Key words: spectrum filter, fully constrained unmixing, mixture analysis, multispectral/hyperspectral remote sensing

CLC number: TP751.1 **Document code:** A

Citation format: Mei S H, He M Y. 2010. A novel spectrum filter for fully constrained mixture analysis. *Journal of Remote Sensing*. **14**(1): 068—079

1 INTRODUCTION

Multispectral/hyperspectral remote sensing, which can generate images with abundant spectral information, has been widely utilized in many applications such as mineral detection (Banerji *et al.*, 1998), archaeology research (Ware *et al.*, 2000), land cover mapping (Tatem *et al.*, 2003), vegetation investigation (Lee *et al.*, 2004), and etc. (Yang *et al.*, 2003). Generally, spectral sensors are deployed on either aircrafts or satellites and images are acquired in low spatial resolution. As a result, pixels in a remote sensing image usually contain more than one surface component, which are often known as "mixed pixels" or "mixtures". Therefore, the traditional classification algorithms, which assign each pixel in an image to only one category of ground object, can not provide accurate interpretation for the remote sensing images. Such a problem can be solved by precisely obtaining the exact distributions of ground objects, which is known as "Mixed Pixel Unmixing" or "Mixture Analysis" (Han *et al.*, 2004). The accurate decomposition of mixtures is of crucial importance for the quantitative analysis of remote sensing images, and also plays an extremely important role in sub-pixel based target diction and classification application.

The model for mixtures has been summarized into the following five categories (Ichoku *et al.*, 1996): the Linear Mixture Model (LMM), the Probabilistic Model, the Geometric Model, the Stochastic Geometric Model, and the Fuzzy Model, in which the LMM has been widely utilized in real applications due to its effectiveness and simplicity. Many LMM based unmixing algorithms have been proposed for target detection, object identification, classification, quantification, and etc. Zhu (1995) solved the LMM by least square methods for mixture classification. Harsanyi & Chang (1994) and Chang *et al.* (1997, 2005) utilized orthogonal subspace projection (OSP) based mixture analysis methods for hyperspectral classification, dimensionality reduction and feature extraction. Chang *et al.* (1998) applied the oblique subspace projection to mixed pixel classification. However, these algorithms may generate minus abundance for ground objects, which is physically meaningless to reflect the ground truth. Therefore, it is impossible to apply them to the quantitative analysis of remote sensing images. Although the Fully Constrained Least Square (FCLS) algorithm utilizes iterative method to eliminate the minus abundance for ground objects (Heinz *et al.*, 1999, 2001), the accuracy of the unmixing results need to be further improved. In this paper, a spectrum filter, which could wipe off the background spectrum in mixtures to obtain the sum-to-one constrained abundance, is proposed. By utilizing the proposed spectrum filter process mixtures iteratively, the physically meaningless minus abundance can be eliminated. Thus, the fully constrained mixture analysis achieves. Finally, the performance of the proposed algorithm is demonstrated on both synthetic and real remote sensing data sets.

Received: 2008-12-25; **Accepted**: 2009-01-05

Foundation: National Natural Science Foundation of China (No. 60572097 and No. 60736007), and NPU base research plan.

First author biography: MEI Shao-hui (1984—), male, PhD candidate of Signal and Information Processing in Northwestern Polytechnical University. His main research area is remote sensing data processing. E-mail: meishaohui@gmail.com

2 LINEAR MITURE MODEL

Due to the spatial resolution limitation, mixed pixels, which contain energy reflected from more than one type of ground object, are inevitably presented in remote sensing images. In the LMM, as shown in Fig.1, the photons reflected from different ground objects contained in one pixel are assumed not to interfere with each other. As a result, the reflected spectrum is a weighted linear sum of the spectrum reflected from inhomogeneous materials. Generally, the spectrums of typical constituent ground objects in a mixed pixel are known as "endmember" and their corresponding proportions are known as "abundance". Therefore, the mixed pixel of a mixture equals to the linear combination of endmember contained in it and their corresponding abundance.

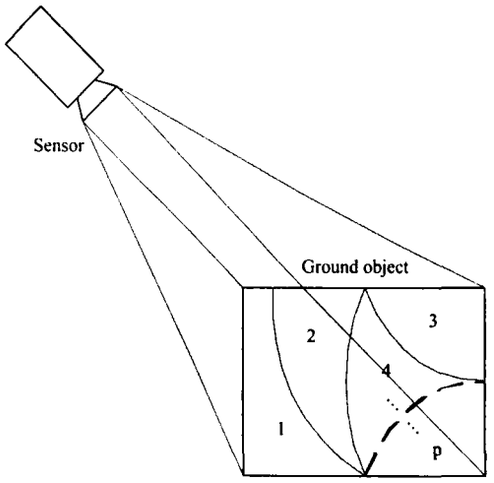

Fig. 1 Sketch map of the satellite remote sensing

Let $\boldsymbol{r}=(r_1,r_2,\cdots,r_b)^{\mathrm{T}}$ be a mixed pixel vector, where b is the number of bands. Let $\boldsymbol{M}=(\boldsymbol{m}_1,\boldsymbol{m}_2,\cdots,\boldsymbol{m}_p)$ be the endmember matrix, in which $\boldsymbol{m}_j=(m_{1j},m_{2j},\cdots,m_{bj})^{\mathrm{T}}$ ($j=1,2,\cdots,p$) is a $b\times1$ column vector representing the j-th endmember spectrum and p is the number of the spectrums of interest. Let $\boldsymbol{\alpha}=(\alpha_1,\alpha_2,\cdots,\alpha_p)^{\mathrm{T}}$ be the corresponding abundance vector, where a_j is the abundance of the j-th spectrum in the mixed pixel. Based on the linear mixing theory aforementioned, the spectrum of a mixed pixel can be represented by a linear regression model as follows,

$$\boldsymbol{r}=\boldsymbol{M}\boldsymbol{\alpha}+\boldsymbol{n}=\sum_{j=1}^{p}\boldsymbol{m}_j\alpha_j+\boldsymbol{n}, \tag{1}$$

where $\boldsymbol{n}$ is a $b\times1$ column vector representing Gaussian noise. Its average is zero and variance is $\sigma^2\boldsymbol{I}$, in which $\boldsymbol{I}$ is a unit matrix.

In order to make the LMM more precise and scientific to describe mixed pixels, the Sum-to-one constraint and the Nonnegative constraint must be imposed on the LMM, which can be expressed as follows,

$$\sum_{j=1}^{p}\alpha_j=1, \tag{2}$$

$$\alpha_j\geqslant0\quad j=1,2,\cdots,p \tag{3}$$

The Sum-to-one constraint is imposed since all the constituent proportions form one pixel; while the Nonnegative constraint is imposed because the negative abundance is physically meaningless to reflect the ground truth.

3 FULLY CONSTRAINED MIXTURE ANALYSIS BY SPECTRUM FILTER

3.1 The construction of spectrum filter

Generally, the spectrum of a pixel can be considered to be composed by the following three part (Tung *et al.*, 2001),

$$\boldsymbol{r}=\boldsymbol{S}+\boldsymbol{B}+\boldsymbol{n}, \tag{4}$$

in which $\boldsymbol{S}$ represents the signal spectrum, $\boldsymbol{B}$ represents the background spectrum, and $\boldsymbol{n}$ represents noise. According to the LMM defined by Eq. (1), we have,

$$\boldsymbol{S}+\boldsymbol{B}=\boldsymbol{M}\boldsymbol{\alpha}. \tag{5}$$

Therefore, both the signal spectrum and the background spectrum are results of endmember spectrum. In order to obtain the abundance of a typical ground object, the space generated by endmembr can be devided into the signal spectrum subspace and the background spectrum subspace, in which the signal spectrum subspace is generated by the spectrum of interest and the background spectrum subspace is generated by the other $p-1$ spectrums contained in the endmember set. Let $\boldsymbol{m}_s$ ($b\times1$ dimensional column vector) be the signal endmember spectrum vector whose corresponding abundance is represented by α_s, and let $\boldsymbol{M}_b$ ($b\times(p-1)$ dimensional matrix) represents the background endmember spectrum matrix and their corresponding abundance is denoted by $\boldsymbol{\alpha}_b$. Consequently, the signal spectrum and the background spectrum are generated by their corresopnding endmember spectrum as follows,

$$\boldsymbol{S}=\boldsymbol{m}_s\alpha_s, \tag{6}$$

$$\boldsymbol{B}=\boldsymbol{M}_b\boldsymbol{\alpha}_b. \tag{7}$$

Therefore, the LMM defined by Eq. (1) can be rewriten as follows,

$$\boldsymbol{r}=\boldsymbol{m}_s\alpha_s+\boldsymbol{M}_b\boldsymbol{\alpha}_b+\boldsymbol{n}. \tag{8}$$

In order to obtain the abundcance of signal spectrum, a spectrum filter $\boldsymbol{k}$ ($1\times b$ dimensional column vector) is proposed to directly eliminate the background spectrum from the pixel vector, which satisfies,

$$\begin{cases}\boldsymbol{k}\boldsymbol{m}_s=\gamma & \gamma\in R\\ \boldsymbol{k}\boldsymbol{M}_b=\boldsymbol{0}_{p-1}\end{cases}, \tag{9}$$

in which $\boldsymbol{0}_{p-1}$ represents the $p-1$ dimensional zero vector. If the spectrum filter is applied to the LMM defined Eq. (8), we have,

$$\boldsymbol{k}\boldsymbol{r}=\boldsymbol{k}\boldsymbol{m}_s\alpha_s+\boldsymbol{k}\boldsymbol{M}_b\boldsymbol{\alpha}_b+\boldsymbol{k}\boldsymbol{n}=\gamma\alpha_s+\boldsymbol{k}\boldsymbol{n}. \tag{10}$$

Therefore, the abundance of signal spectrum is,

$$\alpha_s=\frac{\boldsymbol{k}\boldsymbol{r}}{\gamma}-\frac{\boldsymbol{k}\boldsymbol{n}}{\gamma}. \tag{11}$$

If the Gaussion noise contained in the pixel is ignored, which can be achieved by denoising the images previously, the abun-

dance of signal spectrum is,

$$\alpha_s = \frac{\boldsymbol{kr}}{\gamma}. \tag{12}$$

3.2 The solving of spectrum filter

The sum-to-one constraint can be embedded into the LMM to form a sum-to-one constrained LMM expressed as follows:

$$\begin{pmatrix} r_1 \\ \vdots \\ r_b \\ \delta \end{pmatrix} = \begin{pmatrix} m_{11} & \cdots & m_{1p} \\ \vdots & \ddots & \vdots \\ m_{b1} & \cdots & m_{bp} \\ \delta & \cdots & \delta \end{pmatrix} \times \begin{pmatrix} \alpha_1 \\ \vdots \\ \alpha_p \end{pmatrix} + \begin{pmatrix} n_1 \\ \vdots \\ n_p \\ 0 \end{pmatrix}, \tag{13}$$

in which δ is the trade-off between the LMM and the sum-to-one constraint. If the spectrum filer is constructed on the basis of the sum-to-one constrained LMM defined by Eq. (13), the unmixing results obtained by the proposed spectrum filer will satisfy the sum-to-one constraint.

In terms of the abundance sum-to-one constraint, the spectrum filter, signal spectrum, and background spectrum can be revised as follows,

$$\boldsymbol{k}' = (\boldsymbol{k} \quad 1), \tag{14}$$

$$\boldsymbol{m}_s' = \begin{pmatrix} \boldsymbol{m}_s \\ \delta \end{pmatrix}, \boldsymbol{M}_b' = \begin{pmatrix} \boldsymbol{M}_b \\ \delta \cdot \mathbf{1}_{p-1}^{\mathrm{T}} \end{pmatrix}, \tag{15}$$

where $\mathbf{1}_{p-1}$ is a $p-1$ dimensional column vector contains all ones. If these revisional items are adopted to replace the corresponding items in Eq. (9), the unmixing results obtained by the spectrum filter will satisfy the sum-to-one constraint,

$$\begin{cases} \boldsymbol{k}'\boldsymbol{m}_s' = \gamma \\ \boldsymbol{k}'\boldsymbol{M}_b' = \mathbf{0}_{p-1} \end{cases}. \tag{16}$$

Consequently, in terms of the abundance sum-to-one constraint, the spectrum satisfies (substitute Eq. (14) and Eq. (15) into Eq. (16)),

$$\begin{cases} \boldsymbol{k}\boldsymbol{m}_s = \gamma - \delta \\ \boldsymbol{k}\boldsymbol{M}_b = -\delta \cdot \mathbf{1}_{p-1} \end{cases}. \tag{17}$$

Let $\gamma = \delta$, we have,

$$\boldsymbol{k}\boldsymbol{m}_s = 0. \tag{18}$$

Since the endmember spectrum is consist of signal endmember spectrum and background endmember spectrum, which means $\boldsymbol{M} = (\boldsymbol{m}_s \ \boldsymbol{M}_b)$, Eq. (17) can be rewritten as follows,

$$\boldsymbol{k}\boldsymbol{M} = \delta \boldsymbol{O}, \tag{19}$$

where,

$$\boldsymbol{O} = (0, -1, \cdots, -1). \tag{20}$$

If $p \geqslant b$, which means the number of bands is not larger than the number of ground objects, Eq. (19) is a determined or over-determined equation. Therefore, the spectrum filter $\boldsymbol{k}$ has least square solution,

$$\boldsymbol{k} = \delta \cdot \boldsymbol{O}\boldsymbol{M}^T (\boldsymbol{M}\boldsymbol{M}^T)^{-1}. \tag{21}$$

If $p<b$, which means the number of bands is larger than the number of ground objects, equation (19) is a under-determined equation. Therefore, the spectrum filter $\boldsymbol{k}$ has lots of solution.

Consequently, the abundance of signal spectrum obtained by utilizing the spectrum filter defined by equation (21) is,

$$\alpha_s = \frac{\gamma}{\delta}\boldsymbol{k}\boldsymbol{r} = \boldsymbol{k}\boldsymbol{r} \tag{22}$$

Since the sum-to-one constraint has been considered in solving the spectrum filter, the unmixing results will satisfy the sum-to-one constraint. In addition, according to Eq. (22), the parameter δ has been eliminated in the unmixing results.

3.3 The fully constrained mixture analysis by spectrum filter

When using the proposed spectrum filer to perform mixture analysis, only the sum-to-one constraint of LMM has been considered. However, the abundace of all typical ground objects can not be ensure to be nonnegative, which means some physically meaningless minus abundance may be generated for some ground objects. Such problem may be caused by adopting some typical ground objects which are actually not contained in this mixture as endmember. Therefore, it is of crucial importance to determine the proper endmember set for a specific mixture analysis.

According to Fully Constrained Least Square (FCLS) algorithm (Heinz *et al.*, 2001), the iterative methods can be adopted to eliminate minus abundance in the unmixing procedure. Therefore, in this paper, the iterative analysis by the proposed spectrum filter is adopted to realize fully constrained mixture analysis. When using the proposed spectrum to perform mixture analysis, all the typical ground objects in an image can be selected as an initial endmember set for all the mixtures in the image. In the unmixing procedure for a specific mixture, the unincluded ground objects can be identified according the unmixing results by the spectrum filter. Hence, a new endmeber set can be constructed for mixture analysis by deleting these unincluded ground objects from the initial endmember set. Consequently, the spectrum filter based unmixing procedure can be perform iteratively according to new endmember set until all of the abundance are nonnegative. In the real applications, the initial endmember set is continually modified by wiping off the spectrum corresponding to the largest minus abundance in the unmixing results. A maximum of $p-1$ iterations are acquired for a specific mixture analysis. Therefore, the spectrum filter based fully constrained mixture analysis algorithm is as follows:

Step 1: Select each spectrum of the typical ground object in the endmember set as signal spectrum to calculate its corresponding abundance according to Eq. (22).

Step 2: If the abundance of all the ground objects are nonnegative, which means $\alpha_j \geqslant 0 (j = 1, 2, \cdots, p)$, the proper unmixing results achieved. Otherwise, turn to Step 3.

Step 3: Find the minus abundance with maxmum absolute value and let it be 0. And then wipp off its corresponding spectrum from endmember space to form a new endmeber set for mixture analysis. Turn to Step 1 to contruct new spectrum filters to perform the mixture analysis again.

4 EXPERIMENTS

In this section, the performance of the proposed spectrum filer based fully constrained mixture analysis is demonstrated.

4.1 Experiments on synthetic multispectral data

In this section, the spectrum of typical ground objects obtained by Landsat-7 satellite is selected as endmember spectrum. The synthetic mixtures are generated according to LMM to compare the proposed Fully Constrained Spectrum Filer (FCSF) based mixture analysis algorithm against the popular Fully Constrained Least Square (FCLS) algorithm (Daniel *et al.*, 2001) and the Orthogonal Subspace Projection (OSP) algorithm (Chang *et al.*, 2005). The spectrums of four ground objects including building, swamp, water, and road, are adopted as endmember spectrum (as shown in Fig. 2). The first mixture is simulated with 100% building and 0% other ground objects. And then in the following mixtures, the building is decreased by 1% each pixel until the 100th mixture containing only 1% building. Correspondingly, the other components of swamp, water, and road totally increase by the increment of 1%, where the increment ratio among them is 5:3:2, which means the swamp increases from 0 to 50% by the increment of 0.5%, the water increases from 0 to 30% by the increment of 0.3%, and the swamp increases from 0 to 20% by the increment of 0.2%. Totally 100 mixtures are simulated. In addition, White Gaussian noise is added to these mixtures to make the simulation more authentic to simulate the real situation.

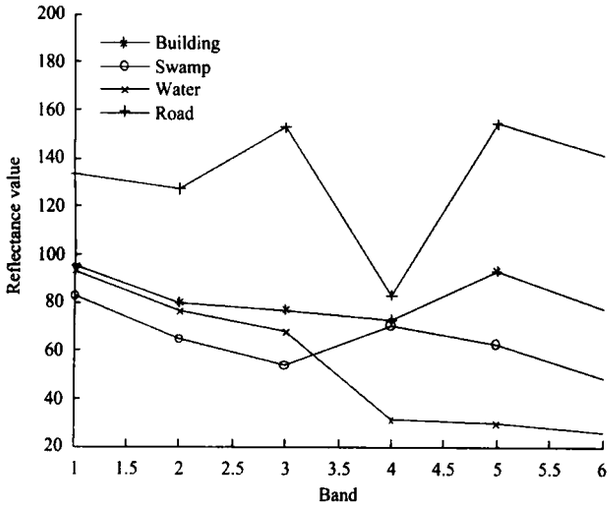

Fig. 2 Spectrum of four typical ground objects obtained by Landsat-7 Satellite

Table 1 Decomposition results of the three algorithms (SNR=10dB)

	RMSE	CC	Time consumption /s
FCSF	**0.0299**	**0.9842**	0.030
FCLS	0.0432	0.9718	0.023
OSP	0.0310	0.9831	**0.019**

Table 1 tabulates the mixture analysis results of the proposed FCSF, FCLS and OSP algorithms when the Signal-to-Noise Ratio (SNR) level in the synthetic data is 10 dB. The Root Mean Square Error (RMSE) and Correlation Coefficient (CC) are adopted to quantitatively evaluate these algorithms. The computation times by implanting these algorithms on Matlab platform are also listed in Table 1. Deduced from Table 1, the proposed FCSF based mixture analysis algorithm, which achieves the least RMSE and the biggest CC with the real fractional abundance, outperforms the other two algorithms in spite of a little more time consumption. The OSP algorithm spends least computation time of these three algorithms. However, it often generates minus fractions for ground objects, which is physically meaningless to reflect the ground truth. Although it can be utilized to improve the performance of image classification and target recognition, it is impossible to apply it to the quantitative analysis of remote sensing images as the unmixing results often do not reflect the ground truth. The proposed FCSF algorithm confines the fractional abundance to [0, 1], and the sum of them is restricted to one to meet the LMM. Although the FCLS algorithm can also confine the abundance fractions to [0, 1], its unmixing results are inferior to that of the prposed FCSF algorithm at the same SNR level. Therefore, the proposed FCSF algorithm is of great potential in the quantitative analysis of remote sensing images. Fig. 3 shows the RMSE of these three algorithms at different SNR levels. It is observed that the proposed FCSF algorithm is more robust and consistent to noise than the other two algorithms. In addtion, the unmixing results of the proposed FCSF algorithm are much better than that of the other two algorithms especially when the SNR is low.

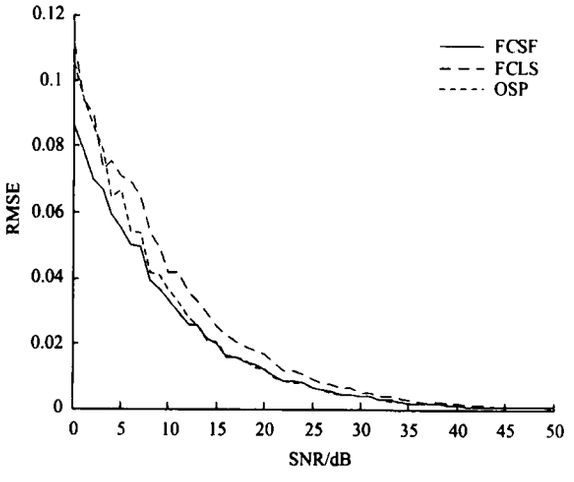

Fig. 3 RMSE of three algorithms at different noise levels

4.2 Experiments with real hyperspectral image

A real hyperspectral scenario of the Jasper Ridge area located in California of USA, collected on Jul 18th, 2000, is utilized to demonstrate the performance of the proposed FCSF

based mixture analysis algorithm. Totally 60 spectral bands covering the spectrum ranging from 441.0nm to 1320.8nm are selected. Fig. 4 shows a Pseudo color image of this area where band 10 is displayed as red, band 20 as green, and band 30 as blue. In this experiment, the spectrum of water, vegetation, road, and two kinds of soils are selected as endmember spectrum for mixture analysis. The decomposition results of the proposed FCSF algorithm, denoted by abundance gray image, are shown in Fig. 5. In these images, pure black denotes that the percentage of the ground objects in the mixture is 0, while pure white denotes 1. Observed from these fractional mapps, two kinds of soil, which are covered by vegetations (as shown in Fig. 5(a)), mainly present in this area (as shown in Fig. 5(d), (e)). A lake exists on the top of this area (as shown in Fig. 5(b)) and a road runs through from righttop to rightdown in this area. Consequently, the proposed FCSF algorithm is of great potential in the intepretation of remote sensing images.

Fig. 4 Pseudo color map of Jasper Ridge (Band 10, 20, 30)

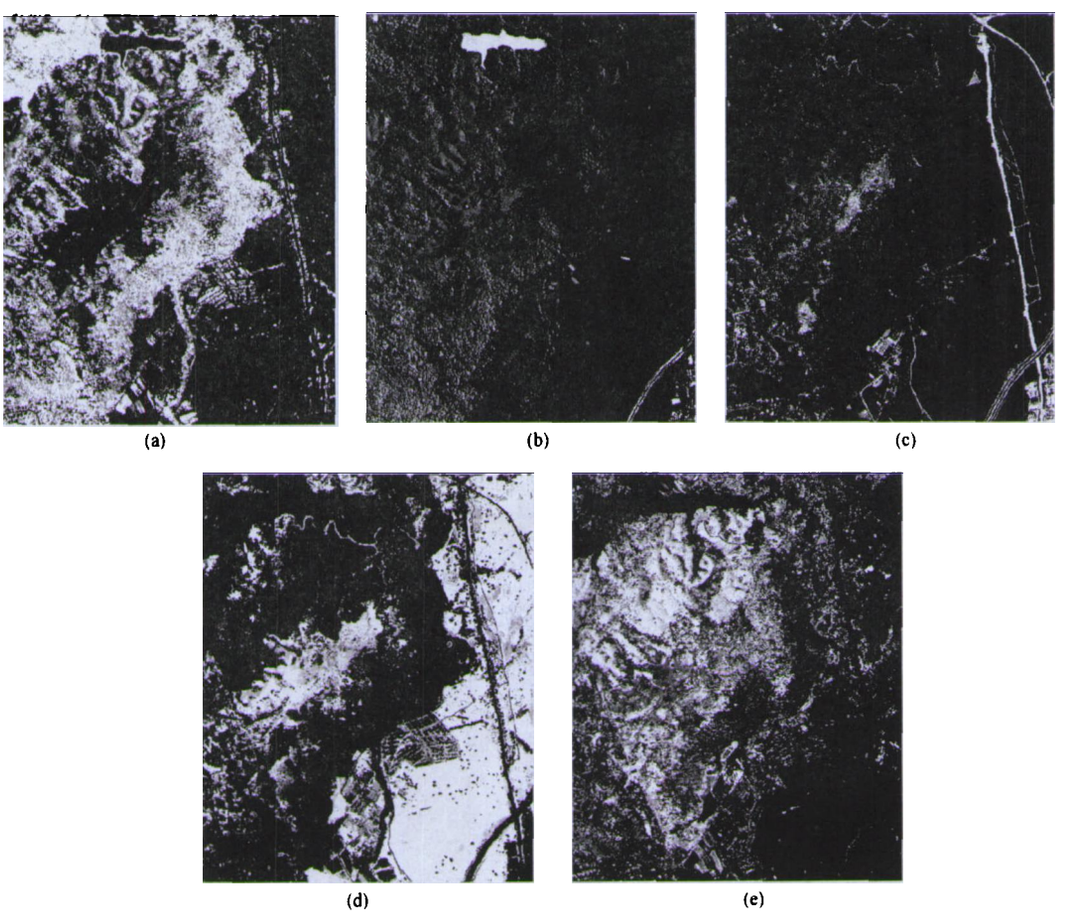

(a) (b) (c) (d) (e)

Fig. 5 Fractional images of Jasper Ridge area
(a) Vegetation; (b) Water; (c) Road; (d) Soil 1; (e) Soil 2

5 CONCLUSION

A spectrum filter, which can directly obtain the abundance of ground objects by wiping off the background spectrum from mixture spectrum, is constructed in this paper. In addition, the fully constrained mixture analysis algorithm based on the proposed spectrum filter is also presented. Experimental results demonstrate that the proposed mixture analysis algorithm can generate accurate fractional abundance maps for remote sensing images, indicating that the proposed FCSF mixture analysis algorithm can be utilized not only to perform the quantitative analysis of remote sensing images, but also to improve the performance of image classification and target recognition.

REFERENCES

Banerji A and Goutsias J A. 1998. Morphological approach to automatic mine detection problems. *IEEE Transactions* on Aerospace and Electronic Systems, **34**: 1085—1096

Chang C I, Zhao X L, Althouse M L G and Pan J J. 1998. Least squares subspace projection approach to mixed pixel classification for hyperspectral images. *IEEE Transactions on Geoscience and Remote sensing*, **36**(3): 898—912

Chang C I. 2005. Orthogonal subspace projection (OSP) revisited: a comprehensive study and analysis. *IEEE Transactions on Geoscience and Remote sensing*, **43**(3): 502—518

Han J H, Huang D S, Sun Z L and Cheung Y M. 2004. A novel mixed pixels unmixing method for multispectral images. *IEEE International Joint Conference on Neural Networks*, **4**: 2541—2545

Harsanyi J C and Chang C I. 1994. Hyperspectral image classification and dimensionality reduction: An orthogonal subspace projection. *IEEE Transactions on Geoscience and Remote sensing*, **32**: 779—785

Heinz D C and Chang C I. 2001. Fully constrained least squares linear spectral mixture analysis method for material quantification in hyperspectral imagery. *IEEE Transactions on Geoscience and Remote sensing*, **39**(3): 529—545

Heinz D C, Chang C I and Althouse M L G. 1999. FuIly constraid least-squares based linear unmixing. *IEEE Geoscience and Remote Sensing Symposium*, **2**: 1401—1403

Ichoku C and Karnieli A. 1996. A review of mixture modeling techniques for sub-pixel land cover estimation. *Remote Sensing Reviews*, **13**: 161—186

Lee J T, Shuai Y M and Zhu Q J. 2004. Using images combined with DEM in classifying forest vegetations. *IEEE Geoscience and Remote Sensing Symposium*, **4**: 2362—2364

Tatem A J, Lewis H G, Atkinson P M and Nixon M S. 2003. Increasing the spatial resolution of agricultural land cover maps using a Hopfield neural network. *International Journal of Geographical Information Science*, **17**(7): 647—672

Tu T M, Chen C H and Chang C I. 1997. A least squares orthogonal subspace projection approach to desired signature extraction and detection. *IEEE Transactions on Geoscience and Remote sensing*, **35**(1): 127—139

Tung C T, Tseng D C and Tsai Y L. 2001. Mixed-pixel classification for hyperspectral images based on multichannel singular spectrum analysis. IEEE Geoscience and Remote Sensing Symposium, **5**: 2370—2372

Ware G A, Chabries D M, Christiansen R W, Brady J E and Martin C E. 2000. Multispectral analysis of ancient maya pigments: implications for the naj tunich corpus. IEEE Geoscience and Remote Sensing Symposium, **6**: 2489—2491

Yang H Z, Han J F, Gong D P and Li Z X. 2003. The development and application of Hyperspectral Remote-Sensing Technology. *Hydrographic Surveying and Charting*, **23**(6): 55—58

Zhu S L. 1995. The classification of remotely-sensed images with mixels. *Journal of the PLA Institute of Surveying and Mapping*, 12(4): 276—278

基于光谱滤波器的混合像元分析

梅少辉, 何明一

西北工业大学 电子信息学院, 陕西省信息获取与处理重点实验室, 陕西 西安 710129

摘 要: 提出一种利用光谱滤波器进行遥感图像混合像元全约束分解的新算法。该算法利用端元光谱中与背景光谱正交的光谱成分构建光谱滤波器, 滤除混合像元中的背景干扰成分, 直接获取信号光谱的丰度。采用该光谱滤波器多次迭代分解, 修正单个混合像元的端元光谱空间, 获取其确切的端元光谱配置, 保证了分解时各端元丰度的非负性, 实现混合像元的全约束分解。多光谱数据仿真实验证明, 与全约束最小二乘法(FCLS)和正交投影(OSP)分解法相比, 该方法虽然在时间方面略逊一点, 但其分解结果与实际结果的相关系数高, 均方根误差小, 具有很高的分解精度, 在遥感定量分析方面具有重要的应用潜力。最后给出了该算法在真实的高光谱图像中进行混合像元分析的结果。

关键词: 光谱滤波器, 全约束分解, 混合像元分析, 多光谱/高光谱遥感

中图分类号: TP751.1 **文献标识码:** A

引用格式: 梅少辉, 何明一. 2010. 基于光谱滤波器的混合像元分析. 遥感学报, 14(1): 068—079

Mei S H, He M Y. 2010. A novel spectrum filter for fully constrained mixture analysis. *Journal of Remote Sensing*. 14(1): 068—079

1 引 言

多/高光谱影像具有丰富的光谱信息, 广泛应用于植被精细分类(Lee 等, 2004)、地矿识别(Tatem 等, 2003)、考古研究(Ware 等, 2000)、月壤分类以及重要目标识别(Banerji 等, 1998)等众多领域(Yang 等, 2003), 其数据处理技术已成为目前遥感技术与应用领域研究的热门课题。由于多/高光谱影像的空间分辨率通常比较低(例如 NASA 的 Landsat 卫星图像的空间分辨率为 900m^2, NOAA-7 卫星图像的空间分辨率为 1.2km^2), 影像上的单个像元通常对应于地面上多种地物成分, 这样的像元通常被称为混合像元。在这种情况下, 传统的将一个像元仅归结到一类地物的分类方法就不能准确地对遥感影像进行解译(Han 等, 2004), 这个问题可以通过获得像元中各类地物的确切含量即混合像元分解来解决。混合像元的精确分解是制约遥感影像定量化应用的一个关键问题, 在多/高光谱图像的亚像元分类和地物目标识别等应用中有着非常重要的作用。

Ichoku 等(1996)将像元的混合模型归结为 5 种类型: 线性模型、概率模型、几何光学模型、随机几何模型和模糊分析模型。其中线性模型以其结构简单、物理含义明确等优点被广泛应用, 多种基于线性模型的混合像元分解方法广泛用于多/高光谱图像地物分类和目标检测与识别等具体应用中, 例如: 朱述龙(1995)使用最小二乘法进行混合像元分类; Harsanyi, Tu 和 Chang 等(1994, 1997, 2005)应用正交子空间投影进行高光谱图像分类、降维以及特征提取; Chang 等(1998)把斜投影应用到混合像元分解中, 进行地物分类处理。但这些算法忽略了特征地物含量的非负性, 其分解结果中存在没有物理意义的负丰度值, 在遥感图像的定量分析方面具有很大的局限性。Heinz 等(1999, 2001)提出的全约束最小二乘分解算法(FCLS), 使用迭代的方法解决了最小二乘分解中存在负系数的问题, 但其分解精度有待提高。本文借助投影理论的思想, 构建一种可以滤除混合像元中背景光谱成分的光谱滤波器。利用该滤波器进行混合像元分析, 可以直接获取信号组

收稿日期: 2008-12-25; **修订日期:** 2009-01-05

基金项目: 国家自然科学基金(编号: 60572097, 60736007), NPU 基础研究计划。

第一作者简介: 梅少辉(1984—), 男, 信号与信息处理学科在读博士生, 2007 年 11 月获得教育部留学基金支持, 进入与悉尼大学联合培养博士计划。主要从事遥感数据处理研究。E-mail: meishaohui@gmail.com。

分的丰度，并且保证混合像元中所有地物的丰度和为 1。此外，利用该滤波器进行迭代分解，可以获取单个混合像元确切的端元光谱配置，确保所有的地物的丰度的非负性。通过基于仿真和真实遥感图像数据的混合像元分析实验验证了该算法的有效性。

2 线性混合模型

遥感图像中混合像元的成像示意图如图 1，混合像元中包含着多种地物目标的信息，是多种纯净地物光谱相互作用的结果。线性混合模型假设像元的光谱响应是该像元包含的所有纯净地物特征光谱的线性组合。一般情况下，遥感图像中纯净地物的特征光谱称为端元光谱，这些端元光谱在混合像元中所占的比例称为丰度。混合像元的光谱响应等于端元光谱及其丰度乘积的累加。

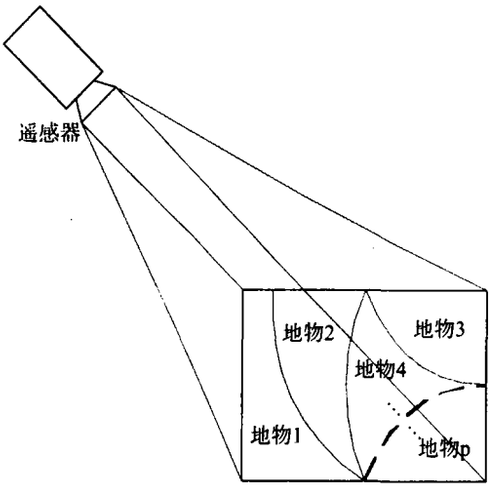

图 1 遥感影像中混合像元成像示意图

记 $\boldsymbol{r}=(r_1,r_2,\cdots,r_b)^{\mathrm{T}}$ 为多/高光谱图像中的混合像元向量，$\boldsymbol{M}=(\boldsymbol{m}_1,\boldsymbol{m}_2,\cdots,\boldsymbol{m}_p)$ 为纯净地物光谱组成的端元矩阵，其中，$\boldsymbol{m}_j=(m_{1j},m_{2j},\cdots,m_{bj})^{\mathrm{T}}$，$(j=1,2,\cdots,p)$ 表示第 j 种端元的特征光谱向量，b 为波段数目，p 为该像元包含的端元的数目；记 $\boldsymbol{\alpha}=(\alpha_1,\alpha_2,\cdots,\alpha_p)^{\mathrm{T}}$ 为 $p\times1$ 维丰度向量，其中 a_j 表示混合像元 $\boldsymbol{r}$ 中第 j 种端元光谱的丰度。根据线性混合原理，混合像元 $\boldsymbol{r}$ 的光谱响应可以通过式(1)所示线性回归模型来表示。

$$\boldsymbol{r}=\boldsymbol{M}\boldsymbol{\alpha}+\boldsymbol{n}=\sum_{j=1}^{p}\boldsymbol{m}_j\alpha_j+\boldsymbol{n} \tag{1}$$

其中，$\boldsymbol{n}$ 表示高斯白噪声，其均值为 0，方差为 $\sigma^2\boldsymbol{I}$，$\boldsymbol{I}$ 是单位阵。

由于这些地物组分构成一个混合像元，所以其丰度和为 1：

$$\sum_{j=1}^{p}\alpha_j=1 \tag{2}$$

并且，所有丰度必须大于 0，即：

$$\alpha_j\geqslant0\quad j=1,2,\cdots,p \tag{3}$$

3 基于光谱滤波器的混合像元全约束分解

3.1 光谱滤波器的构造

像元 $\boldsymbol{r}$ 的特征光谱可以看作是以下几部分的和(Tung 等, 2001)：

$$\boldsymbol{r}=\boldsymbol{S}+\boldsymbol{B}+\boldsymbol{n} \tag{4}$$

其中，$\boldsymbol{S}$ 表示信号光谱，$\boldsymbol{B}$ 表示背景光谱，$\boldsymbol{n}$ 表示噪声。参照式(1)所示的线性混合模型可知，

$$\boldsymbol{S}+\boldsymbol{B}=\boldsymbol{M}\boldsymbol{\alpha} \tag{5}$$

即信号光谱和背景光谱均由端元光谱生成。为了提取出某一种特征地物的丰度，将由端元光谱张成的空间分解成信号光谱子空间和背景光谱子空间，其中信号光谱子空间由这种地物的特征光谱张成，背景光谱子空间由端元光谱中剩余的 $p-1$ 种纯净地物的特征光谱张成。记 $\boldsymbol{m}_s$($b\times1$ 维列向量)为信号端元光谱向量，对应的丰度为 α_s；$\boldsymbol{M}_b$($b\times(p-1)$维矩阵)为背景端元光谱矩阵，对应的丰度向量为 α_b($(p-1)$维列向量)，则信号光谱和背景光谱分别可以表示为：

$$\boldsymbol{S}=\boldsymbol{m}_s\alpha_s \tag{6}$$

$$\boldsymbol{B}=\boldsymbol{M}_b\alpha_b \tag{7}$$

于是式(1)所示的线性混合模型可以改写为：

$$\boldsymbol{r}=\boldsymbol{m}_s\alpha_s+\boldsymbol{M}_b\alpha_b+\boldsymbol{n} \tag{8}$$

为了求出信号光谱的丰度 α_s，本文构造一个可以直接从像元中滤除背景光谱的光谱滤波器 $\boldsymbol{k}$($1\times b$ 维行向量)，令其满足：

$$\begin{cases}\boldsymbol{k}\boldsymbol{m}_s=\gamma & \gamma\in R\\ \boldsymbol{k}\boldsymbol{M}_b=\boldsymbol{0}_{p-1}\end{cases} \tag{9}$$

其中 $\boldsymbol{0}_{p-1}$ 为 $p-1$ 维零向量。对式(8)所示的混合像元模型使用光谱滤波器 $\boldsymbol{k}$ 进行滤波处理可得：

$$\boldsymbol{k}\boldsymbol{r}=\boldsymbol{k}\boldsymbol{m}_s\alpha_s+\boldsymbol{k}\boldsymbol{M}_b\alpha_b+\boldsymbol{k}\boldsymbol{n}=\gamma\alpha_s+\boldsymbol{k}\boldsymbol{n} \tag{10}$$

因此，信号端元的丰度：

$$\alpha_s=\frac{\boldsymbol{k}\boldsymbol{r}}{\gamma}-\frac{\boldsymbol{k}\boldsymbol{n}}{\gamma} \tag{11}$$

如果忽略高斯噪声的影响(对图像进行降噪预处理)，信号光谱的丰度可以表示为：

$$\alpha_s=\frac{\boldsymbol{k}\boldsymbol{r}}{\gamma} \tag{12}$$

3.2 光谱滤波器的求解

考虑到丰度和为 1 的约束，式(1)所示的线性混合模型可以改写为:

$$\begin{pmatrix} r_1 \\ \vdots \\ r_b \\ \delta \end{pmatrix} = \begin{pmatrix} m_{11} & \cdots & m_{1p} \\ \vdots & \ddots & \vdots \\ m_{b1} & \cdots & m_{bp} \\ \delta & \cdots & \delta \end{pmatrix} \times \begin{pmatrix} \alpha_1 \\ \vdots \\ \alpha_p \end{pmatrix} + \begin{pmatrix} n_1 \\ \vdots \\ n_p \\ 0 \end{pmatrix} \tag{13}$$

其中，δ为丰度和为 1 约束的权值。使用该修正的线性模型进行混合像元分析，可以保证各端元光谱的丰度和为 1。

为了方便分析，对光谱滤波器、信号光谱和背景光谱进行如下修正:

$$\boldsymbol{k}' = (\boldsymbol{k} \quad 1) \tag{14}$$

$$\boldsymbol{m}_s' = \begin{pmatrix} \boldsymbol{m}_s \\ \delta \end{pmatrix}, \boldsymbol{M}_b' = \begin{pmatrix} \boldsymbol{M}_b \\ \delta \cdot \mathbf{1}_{p-1}^{\mathrm{T}} \end{pmatrix} \tag{15}$$

其中 $\mathbf{1}_{p-1}$ 为全为 1 的 $p-1$ 维列向量。利用这些修正项替代式(9)中的对应项，可以在滤除背景光谱的同时保证获取的丰度和为 1:

$$\begin{cases} \boldsymbol{k}'\boldsymbol{m}_s' = \gamma \\ \boldsymbol{k}'\boldsymbol{M}_b' = \mathbf{0}_{p-1} \end{cases} \tag{16}$$

考虑了丰度和为 1 的约束后，光谱滤波器应满足(将式(14)和(15)代入式(16)进行化简):

$$\begin{cases} \boldsymbol{k}\boldsymbol{m}_s = \gamma - \delta \\ \boldsymbol{k}\boldsymbol{M}_b = -\delta \cdot \mathbf{1}_{p-1} \end{cases} \tag{17}$$

令$\gamma = \delta$, 则

$$\boldsymbol{k}\boldsymbol{m}_s = 0 \tag{18}$$

并且记

$$\boldsymbol{O} = (0, -1, \cdots, -1) \tag{19}$$

考虑到端元光谱由信号端元光谱和背景端元光谱组成，即 $\boldsymbol{M} = (\boldsymbol{m}_s \ \boldsymbol{M}_b)$，所以式(17)可以改写为:

$$\boldsymbol{k}\boldsymbol{M} = \delta\boldsymbol{O} \tag{20}$$

当 $p \geqslant b$ 时，即图像中地物类别数目大于或等于波段数目时，式(20)为过定或恰定方程，光谱滤波器 $\boldsymbol{k}$ 具有最小二乘解:

$$\boldsymbol{k} = \delta \cdot \boldsymbol{O}\boldsymbol{M}^{\mathrm{T}}(\boldsymbol{M}\boldsymbol{M}^{\mathrm{T}})^{-1} \tag{21}$$

当 $p<b$ 时，即图像中地物类别数目小于波段数目时，式(20)为欠定方程，光谱滤波器 $\boldsymbol{k}$ 具有无数个解，只需取其中任一解即可。

于是信号光谱的丰度:

$$\alpha_s = \frac{\gamma}{\delta}\boldsymbol{k}\boldsymbol{r} = \boldsymbol{k}\boldsymbol{r} \tag{22}$$

由于使用嵌入了丰度和为 1 约束的修正混合模型求解光谱滤波器，所以求得的丰度满足和为 1 的约束。此外，从式(22)可以看出，使用该光谱滤波器进行混合像元分解时，消除了权值δ对结果的影响。

3.3 混合像元的全约束分解

使用光谱滤波器进行混合像元分解时，仅仅考虑了丰度和为 1 的约束，不能保证所有特征地物的丰度的非负性，即在分解时可能会产生一些没有物理意义的负的丰度值，这可能是由于该像元中并不包含当前分解时所采用的端元光谱组合中的某些地物成分造成的，也就是说，在进行混合像元分解时，采用的端元光谱数多于该像元中实际包含的端元光谱数。所以，确保丰度值非负的关键就是获取该像元的准确的端元光谱配置。

根据 Heinz 等(1999, 2001)人提出的全约束最小二乘线性分解的思想，采用迭代分解的方法，可以获取混合像元确切的端元光谱配置，保证获取的地物丰度的非负性。于是，在使用本文提出的光谱滤波器法进行混合像元分解时，可以采用迭代分解的方法，从分解结果中找出该像元不包含的端元光谱，将其从端元光谱空间中删除，对端元光谱空间进行修正，然后利用基于新的端元光谱空间的光谱滤波器进行分解，直到获取的所有地物成分的丰度值非负为止。具体操作时，从分解结果中找出绝对值最大的负丰度值，令其为0，并将其对应的端元光谱从当前的端元光谱矩阵中删除，构建新的端元光谱矩阵，产生新的光谱滤波器重新进行分解，重复这一过程，直到获取的所有地物的丰度值均非负为止。该算法最多需要迭代 $p-1$ 步，当不需要进行丰度调节时迭代结束。综上所述，利用本文提出的光谱滤波器进行混合像元全约束分解的步骤如下:

(1) 分别将端元光谱空间中的各纯净地物的特征光谱作为信号光谱，利用本文提出的光谱滤波器算法计算混合像元中各纯净地物的丰度值(式(22));

(2) 如果所有地物成分的丰度值均非负，即 $\alpha_j \geqslant 0 (j = 1, 2, \cdots, p)$，则得到正确的分解结果，结束迭代；否则，转向步骤(3);

(3) 找出绝对值最大的负丰度，记为 $\hat{\alpha}$，令 $\hat{\alpha} = 0$，并将其对应的端元光谱向量 $\boldsymbol{m}$ 从原来的端元光谱矩阵 $\boldsymbol{M}$ 中删掉，产生新的端元光谱矩阵 $\boldsymbol{M}'$，然后转向步骤(1)，重新进行混合像元分析。

4 实验结果与分析

4.1 模拟像元实验

该实验采用Landsat-7卫星获取的4种地物的特征光谱作为端元光谱，根据线性混合模型模拟多光

谱像元，用来比较全约束光谱滤波器法(FCSF)与全约束最小二乘分解(FCLS)(Heinz 等，2001)和正交投影分解(OSP)(Chang 等，2005)等算法的性能。其中，端元光谱由水体、建筑物、湿地和公路 4 种纯净地物的特征光谱组成，其特征光谱如图 2。进行多光谱像元仿真时，建筑物的丰度以 0.01 的增量由 1 递减到 0.01，对应的湿地、水体和公路以 5:3:2 的比例增加，并且保证所有的丰度和为 1，即湿地的丰度以 0.005 的增量由 0 递增到 0.495；水体的丰度以 0.003 的增量由 0 递增到 0.297；公路的丰度以 0.002 的增量由 0 递增到 0.198；总共仿真 100 个像元。此外，以一定信噪比在仿真信号时加入高斯噪声，使得仿真的混合像元符合实际情况。

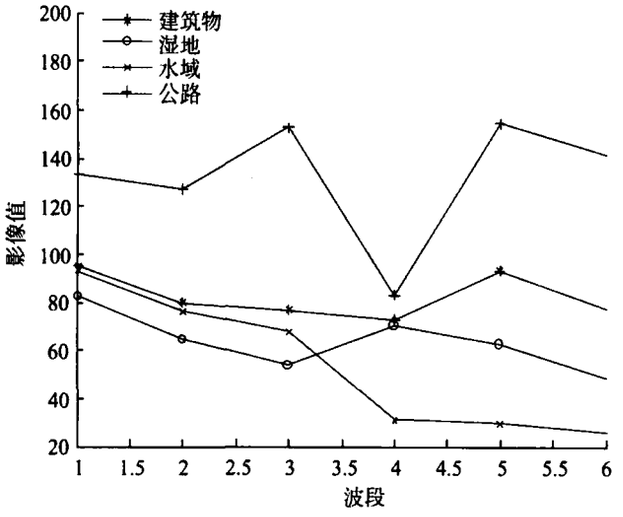

图 2　Landsat-7 卫星获得的 4 种特征地物光谱

表 1　三种分解算法性能比较(信噪比为 10dB)

	均方根误差	相关系数	计算耗时/s
FCSF	**0.0299**	**0.9842**	0.030
FCLS	0.0432	0.9718	0.023
OSP	0.0310	0.9831	**0.019**

表 1 给出了分别利用全约束光谱滤波器(FCSF)法、全约束最小二乘法(FCLS)和正交投影分解法(OSP)进行混合像元分析的结果与真实结果的均方根误差、相关系数以及它们在计算耗时方面的比较。从表 1 看出，全约束光谱滤波器法与真实丰度的均方根误差最小，相关系数最大，均优于其他几种算法，但在时间消耗方面略逊于其他算法。正交投影分解法在分解时往往会生成负投影，产生没有物理意义的负丰度，不符合线性混合模型的约束，与实际情况有一定差异，虽然可以用于遥感图像的亚像元分类和检测等处理，但在遥感图像定量分析方面具有很大的局限性。本文提出的全约束光谱滤波器法获取的各地物成分的丰度均介于 0 和 1 之间，并且所有纯净地物成分的丰度和为 1，符合混合像元的线性模型的约束条件。与全约束最小二乘分解算法相比，在相同的信噪比下，本文提出的全约束光谱滤波器法获得的结果与真实结果的相关系数高，均方根误差小，具有比较高的分解精度，在遥感影像定量分析方面具有很大的应用潜力。图 3 给出了 3 种算法的均方根误差随信噪比变化的曲线图，从图 3 看出，全约束光谱滤波器法对噪声具有一定的抑制作用，在低信噪比情况下的性能明显优于其他两种算法。

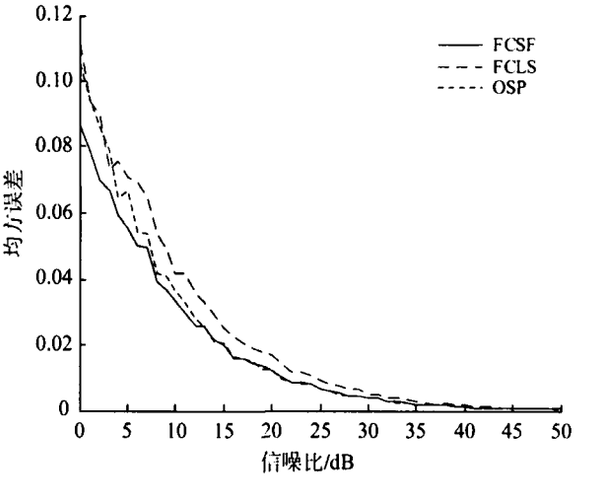

图 3　3 种算法的均方根误差随信噪比变化图

4.2　高光谱图像实验

该实验选取美国加利福尼亚州的 Jasper Ridge 地区的一组 60 波段高光谱影像，波段范围从 441.0—1320.8nm，实验采用全部 60 个波段，其假彩色合成图如图 4。实验选取植被、水域、公路和 2 种质

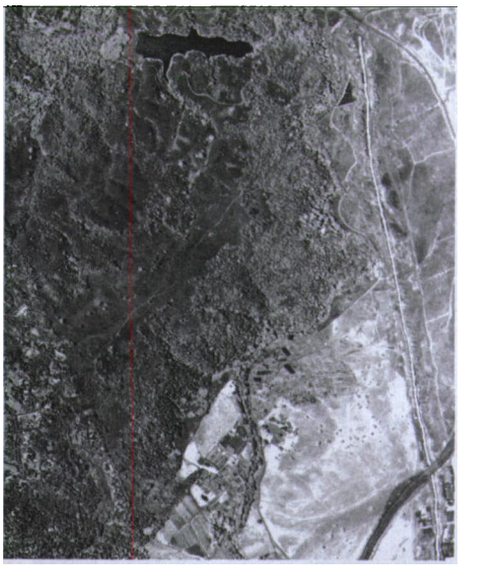

图 4　Jasper Ridge 地区伪彩色图(波段 10, 20, 30)

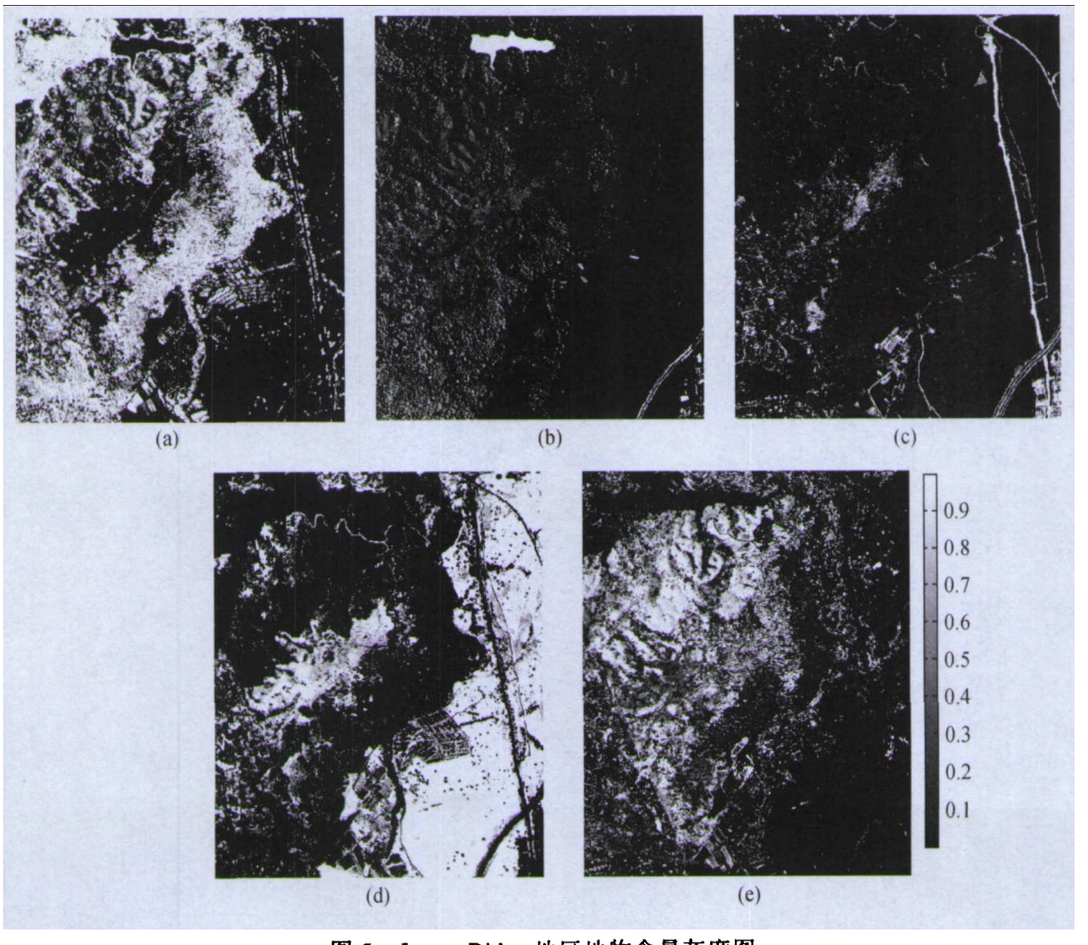

图 5 Jasper Ridge 地区地物含量灰度图

(a) 植被; (b) 水域; (c)公路; (d) 土壤 1; (e) 土壤 2

地不同的土壤的特征光谱作为端元光谱，使用本文提出的全约束光谱滤波器算法进行混合像元分析，分解结果如图 5，其中纯白色代表混合像元中的地物含量为 100%，纯黑色表示其含量为 0。从解译图中可以看出，该区域左边大部分区域为植被覆盖区域(图 5(a))，覆盖着 2 种不同质地的土壤(图 5(d)、(e))，其上方有一块完整的湖泊(图 5(b))，右边自上而下的小窄带为一条道路(图 5(c)中的带状区域)。由此可见，本文提出的基于光谱滤波器的混合像元全约束线性分解算法为遥感图像的解译工作提供有力的支持。

5 结 论

本文构造了一种光谱滤波器，利用该滤波器实现了遥感图像中混合像元的全约束分解。仿真实验证明，该算法的分解结果具有很高的精度，与实际结果的相关系数高，均方根误差小，可直接应用到多光谱和高光谱混合像元分析中。利用该方法进行混合像元分解，不仅可以提高多光谱和高光谱图像分类、目标检测等处理的精度，而且在遥感定量分析方面具有很大的应用潜力。

REFERENCES

Banerji A and Goutsias J A. 1998. Morphological approach to automatic mine detection problems. *IEEE Transactions* on Aerospace and Electronic Systems, **34**: 1085—1096

Chang C I, Zhao X L, Althouse M L G and Pan J J. 1998. Least squares subspace projection approach to mixed pixel classification for hyperspectral images. *IEEE Transactions on Geoscience and Remote sensing*, **36**(3): 898—912

Chang C I. 2005. Orthogonal subspace projection (OSP) revisited: a comprehensive study and analysis. *IEEE Transactions on Geoscience and Remote sensing*, **43**(3): 502—518

Han J H, Huang D S, Sun Z L and Cheung Y M. 2004. A novel mixed pixels unmixing method for multispectral images. *IEEE International Joint Conference on Neural Networks*, **4**: 2541—2545

Harsanyi J C and Chang C I. 1994. Hyperspectral image classification and dimensionality reduction: An orthogonal subspace projection. *IEEE Transactions on Geoscience and Remote*

sensing, **32**: 779—785

Heinz D C and Chang C I. 2001. Fully constrained least squares linear spectral mixture analysis method for material quantification in hyperspectral imagery. *IEEE Transactions on Geoscience and Remote sensing*, **39**(3): 529—545

Heinz D C, Chang C I and Althouse M L G. 1999. FuIly constraid least-squares based linear unmixing. *IEEE Geoscience and Remote Sensing Symposium*, **2**: 1401—1403

Ichoku C and Karnieli A. 1996. A review of mixture modeling techniques for sub-pixel land cover estimation. *Remote Sensing Reviews*, **13**: 161—186

Lee J T, Shuai Y M and Zhu Q J. 2004. Using images combined with DEM in classifying forest vegetations. *IEEE Geoscience and Remote Sensing Symposium*, **4**: 2362—2364

Tatem A J, Lewis H G, Atkinson P M and Nixon M S. 2003. Increasing the spatial resolution of agricultural land cover maps using a Hopfield neural network. *International Journal of Geographical Information Science*, **17**(7): 647—672

Tu T M, Chen C H and Chang C I. 1997. A least squares orthogonal subspace projection approach to desired signature extraction and detection. *IEEE Transactions on Geoscience and Remote sensing*, **35**(1): 127—139

Tung C T, Tseng D C and Tsai Y L. 2001. Mixed-pixel classification for hyperspectral images based on multichannel singular spectrum analysis. IEEE Geoscience and Remote Sensing Symposium, **5**: 2370—2372

Ware G A, Chabries D M, Christiansen R W, Brady J E and Martin C E. 2000. Multispectral analysis of ancient maya pigments: implications for the naj tunich corpus. IEEE Geoscience and Remote Sensing Symposium, **6**: 2489—2491

Yang H Z, Han J F, Gong D P and Li Z X. 2003. The development and application of Hyperspectral Remote-Sensing Technology. *Hydrographic Surveying and Charting*, **23**(6): 55—58

Zhu S L. 1995. The classification of remotely-sensed images with mixels. *Journal of the PLA Institute of Surveying and Mapping*, **12**(4): 276—278

附中文参考文献

杨哲海, 韩建峰, 宫大鹏, 李之歆. 2003. 高光谱遥感技术的发展与应用. 海洋测绘, **23**(6): 55—58

朱述龙. 1995. 基于混合像元的遥感图像分类技术. 解放军测绘学报, **12**(4): 276—278